Received: 5 June 2022 | Accepted: 31 May 2023

DOI: 10.1111/2041-210X.14163

Methods in Ecology and Evolution

RESEARCH ARTICLE

A generalizable normalization for assessing plant functional diversity metrics across scales from remote sensing

Javier Pacheco-Labrador[1] | Francesco de Bello[2,3] | Mirco Migliavacca[1] | Xuanlong Ma[4] | Nuno Carvalhais[1] | Christian Wirth[1,5,6]

[1]Max Planck Institute for Biogeochemistry, Jena, Germany; [2]Centro de Investigaciones sobre Desertificación (CSIC-UV-GV), Valencia, Spain; [3]Department of Botany, University of South Bohemia, České Budějovice, Czech Republic; [4]College of Earth and Environmental Science, Lanzhou University, Lanzhou, China; [5]Systematic Botany and Functional Biodiversity, Leipzig University, Leipzig, Germany and [6]German Centre for Integrative Biodiversity Research (iDiv), Halle-Jena-Leipzig, Germany

Correspondence
Javier Pacheco-Labrador
Email: jpacheco@bgc-jena.mpg.de

Present address
Mirco Migliavacca, European Commission, Joint Research Centre (JRC), Ispra, Italy

Funding information
Comunitat Valenciana, Grant/Award Number: CIAICO/2021/181; Deutsches Zentrum für Luft- und Raumfahrt, Grant/Award Number: 50EE1912; European Space Agency, Grant/Award Number: C.N.4000140028/22/I-DT-lr

Handling Editor: Hooman Latifi

Abstract

1. Remote sensing (RS) increasingly seeks to produce global-coverage maps of plant functional diversity (PFD) across scales. PFD can be quantified with metrics assessing field or RS data dissimilarity. However, their comparison suffers from the lack of normalization approaches that (1) correct for differences in the number and correlation of traits and spectral variables and (2) do not require comparing all the available samples to estimate the maximum trait's dissimilarity (unfeasible in RS).
2. We propose a generalizable normalization (GN) based on the maximum potential dissimilarity for the traits and spectral data considered and compare it to more traditional approaches (e.g. the maximum dissimilarity within datasets). To do so, we simulated plant communities with radiative transfer models and compared RS-based diversity measurements across spatial scales (α- and β-diversity components). Specifically, we assessed the capability of different normalization approaches (GN, local, none) to provide PFD estimates comparable between (1) RS and plant traits and (2) estimates from different RS missions.
3. Unlike the other approaches, GN provides diversity component estimates that are directly comparable between field data and RS missions with different spectral configurations by removing the effect of differences in the number of traits or bands and the maximum dissimilarity across datasets.
4. Therefore, GN enables the separated analysis of RS images from different sensors to produce comparable global-coverage cartography. We suggest GN is necessary to validate RS approaches and develop interpretable maps of PFD using different RS missions.

KEYWORDS
diversity components, diversity partitioning, equivalent numbers, plant functional diversity, radiative transfer model, remote sensing, spectral diversity, spectral variation

1 | INTRODUCTION

Reducing the current biodiversity loss rates requires synoptic, continuous and comparable quantitative biodiversity measurements (Hansen et al., 2021). In this context, remote sensing (RS) emerges as a promising tool for mapping the spatiotemporal variability of vegetation properties at different spatial scales, including biodiversity (Cavender-Bares et al., 2017; Ma et al., 2020; Wang & Gamon, 2019). Among other dimensions of biodiversity, RS could map plant functional diversity (PFD, the variability of plant functional traits), which is a key facet of biodiversity linked to ecosystem functions, stability, and species coexistence (de Bello, Carmona, et al., 2021; De Boeck et al., 2018). This approach is supported by the spectral variation hypothesis, which states that the spectral diversity in an RS image originates from the spatial heterogeneity of the environment, which influences the distribution of plant species and their functional traits (Palmer et al., 2002). PFD can be estimated from the variability of (1) spectral signals (spectral diversity) (Rocchini et al., 2021; Wang, Gamon, Cavender-Bares, et al., 2018) or (2) plant traits (PT) estimated from spectral imagery (e.g. leaf pigments) (Schneider et al., 2017; Torresani et al., 2021). Moreover, PFD can be estimated at local (α, β) or regional (γ) scales, known as biodiversity components (Whittaker, 1972).

Functional diversity metrics (FDMs) summarize the variability of several functional traits (or spectral variables) in a single measure (Mason et al., 2005). They generally require trait standardization and dimensionality reduction (pre-processing) to eliminate collinearity and differences in magnitude across the variables considered (Laliberté & Legendre, 2010). However, pre-processing should be applied to all the samples analysed simultaneously (Botta-Dukát, 2005). This is feasible in local studies (e.g. field surveys) but not in operational RS, where datasets are enormous and continuously grow. Pacheco-Labrador et al. (2022) showed that (1) pre-processing is necessary to link FDMs computed from RS and PT datasets, and (2) separately pre-processing RS images allows comparing some FDMs across images (Rao's quadratic entropy (Q), functional dispersion and functional richness (FRic)). However, differences in the data structure (dimensionality—the number of traits—and collinearity) lead to differences in the FMD values calculated from different datasets (e.g. RS missions), even if these feature similar diversity (Figure S1). This dependency hampers the comparability of PFD estimates, global-scale monitoring, and the use of 'equivalent numbers' in RS (see below).

PFD features different spatial components (i.e. α-, β- and γ-diversity). The correct partitioning of these components likely requires a transformation of these indices, using the so-called 'equivalent numbers' introduced in ecology by Hill (1973) and later by Jost (2006). Equivalent numbers provide formulation-independent values and prevent biases in β-diversity estimation induced by its inherent dependence on α-diversity (Jost, 2007). Their use was initially proposed for indices quantifying taxonomic diversity (species or taxonomical groups), where equivalent numbers were defined as the number of equiprobable species that provide the same index value (Hill, 1973; Jost, 2006). Later works extended their application to indices that account for the traits' dissimilarity between species (Ricotta & Szeidl, 2009), specifically Rao Q (Botta-Dukát, 2005), opening the door to the partitioning of α and β components with functional and phylogenetic variables (de Bello et al., 2010), or spectral data (Rocchini et al., 2018). In this case, the Rao Q equivalent number (Q_{eq}) is the number of equiprobable and maximally dissimilar species that give the same value as the index (Ricotta & Szeidl, 2009). However, calculating Q_{eq} for diversity partitioning requires normalizing the dissimilarity metric within the range [0, 1] to ensure that α is always lower than γ-diversity (de Bello et al., 2010). In ecological studies, this normalization can be achieved by finding the maximum (local) dissimilarity value within the dataset analysed. However, this is not feasible for global RS datasets. So far, RS has evaluated the use of diversity indices (Helfenstein et al., 2022; Torresani et al., 2019; Wang, Gamon, Cavender-Bares, et al., 2018) and partitioning approaches (Khare et al., 2019; Laliberté et al., 2020; Rossi et al., 2021a) such as the total variance framework (Whittaker, 1972) and diversity decomposition (Whittaker, 1960; Whittaker, 1972). However, the potential of equivalent numbers to link RS imagery and PFD remains unexplored.

The lack of accepted normalization approaches for both RS and PT datasets leads to formulation- and data-structure-dependent PFD estimates not directly (1:1) comparable, which limits RS biodiversity-monitoring capabilities. Furthermore, Pacheco-Labrador et al. (2022) showed that self-normalized FDMs (functional divergence or evenness) were not comparable between RS and PT, suggesting that (similar) local normalization might not be suitable in the RS context. Therefore, we propose a generalizable normalization approach (GN) applicable to any dataset of continuous variables and extend it to different metrics and diversity partitioning approaches. Then we use radiative transfer simulations of canopy stands to answer the following research questions: (1) Compared to other non- or local normalization, can GN improve the estimation of PFD from RS? And (2) Can GN make directly (1:1) comparable PFD estimates from RS missions with different spectral configurations?

2 | MATERIALS AND METHODS

To assess the proposed GN, we simulated synthetic communities of species featuring unique PT (Section 2.1) and reflectance factors for different remote sensors using radiative transfer simulations (Figure 1a, Section 2.2). Then, we computed FDMs (Section 2.3) and partitioned diversity components (Section 2.4) from these synthetic

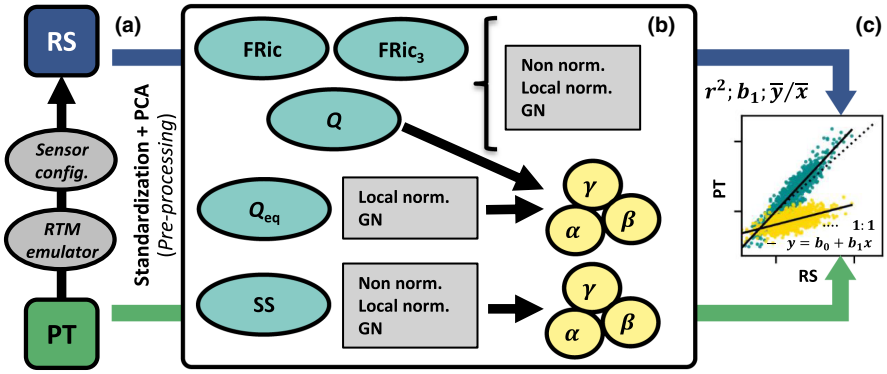

FIGURE 1 Workflow summary. First, a radiative transfer model emulator uses plant traits (PT) featuring species of simulated communities to predict remote sensing (RS) variables (i.e. reflectance factors), which are resampled to the spectral features of different remote sensors (a). Second, PT and RS variables are transformed (standardization and dimensionality reduction with principal component analysis (PCA)) and used to compute different functional diversity indices (functional richness from 8 and 3 principal components and Rao *Q* entropy), Rao *Q* equivalent number (Q_{eq}), and the sum of squares (*SS*). These undergo different normalization levels (non, local, and generalizable (GN)). Then, Rao and *SS* metrics are used to partition α-, β- and γ-diversity components (b). Third, the relationships between metrics and diversity components estimated from RS or PT variables are evaluated using the squared Pearson correlation coefficient, the slope of the linear model, and the averages' ratio (c).

datasets (Figure 1b). Standardization and principal component analysis (PCA) (Pearson, 1901) were first applied to reflectance factors and PT, keeping the components that explained at least 98% of the variance. Eventually, we compared FDMs and diversity components computed from PT and RS datasets with different normalization levels (non, local and generalizable) and sensors' spectral configurations (Section 2.6). GN is described in Section 2.5, whereas 'local normalization' refers to metrics normalized using the maximum value in each dataset representing a region or an RS image.

2.1 | Simulation of synthetic vegetation communities

We simulated 1000 regions (theoretical locations) featuring different community assemblages of synthetic species. Each consists of a species pool (where richness $S_{reg} \epsilon [5, 300]$) distributed in several (between 10 and $S_{reg}/2$) communities (species groups). As in Pacheco-Labrador et al. (2022), these regions have no explicit spatial extent, which we abstracted by working with relative abundances. Following Stier et al. (2016), we used a simple stochastic approach to populate the communities from their regional pool (Figure 2). First, we randomly determined S_{reg} and the relative abundance of species within the pool. Then, we separated the species into random groups, each directly contributing to a part of the communities. However, we allowed a random fraction of other groups' species to contribute to other communities. At this point, we randomly removed species from some communities to increase β-diversity but ensured at least one species per community. Finally, we normalized the relative abundances per community.

As in Pacheco-Labrador et al. (2022), we defined synthetic plant species as sets of radiative transfer model parameters (Table 1) that enable simulating the corresponding reflectance factors. These are used as surrogates of plant functional traits that could be sampled in field surveys (see Pacheco-Labrador et al. (2022) discussion on the suitability of these parameters). We randomly sampled foliar and structural PT within plausible biological bounds ordinary in RS literature and avoided unrealistic combinations by accounting for known covariance between foliar traits (Supporting Information S1). Moreover, to cover the casuistic that assembling mechanisms (e.g. inter and intra-specific interactions, biotic and abiotic filtering) could produce, we forced a fraction of the species pool to feature 'similar' traits and drew the remaining 'dissimilar' species within the broader bounds in Table 1. For example, we could sample chlorophyll content between 40 and 50 or 0 and 100 $\mu g\,cm^{-2}$, respectively. We randomly determined each region's 'similar' species fraction and trait ranges.

The simulated species, communities and regions are respectively represented in RS by pixels, pixel patches or windows, and images (Table S1). We simulated the ideal case where spatial resolution allowed obtaining the spectral signature of individual species (Pacheco-Labrador et al., 2022) and avoided spectral mixture, which is problematic but irrelevant to the normalization itself.

2.2 | Radiative transfer model and emulator

Vegetation radiative transfer models simulate the absorption and scattering of radiation within canopies. They connect leaf biochemical properties (e.g. pigment contents) and canopy structural properties (e.g. leaf area and angles) with the spectral signals measured by remote sensors (Supporting Information S2). Emulators are statistical models (e.g. neural networks) that surrogate physical models at a faster computation speed (Gómez-Dans et al., 2016). We simulated the optical reflectance factors of synthetic species using an emulator of the SCOPE model (v1.73, Matlab 2015b) (van der Tol et al., 2009). The emulator (Scikit-learn v0.2.1, Python 3.7) was trained and

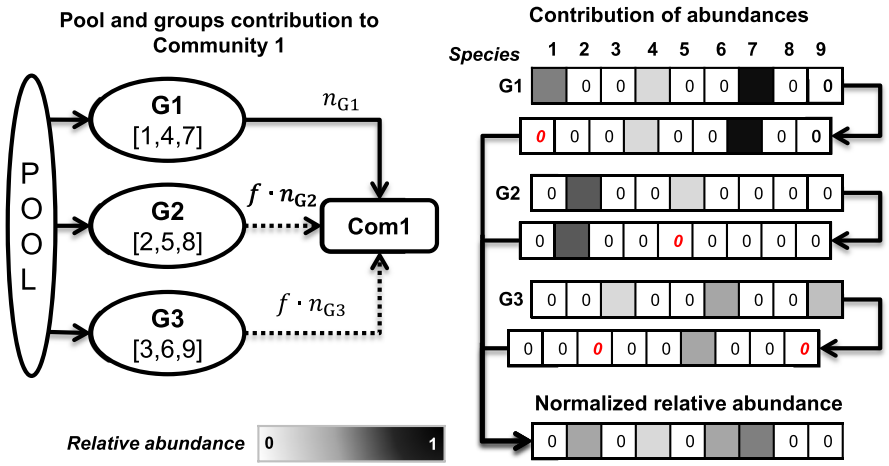

FIGURE 2 Schematic representation of the simulation of one of the communities of a region. Nine species are simulated and labelled from 1 to 9. The species pool is split into three groups (G), not necessarily evenly. Only G1 contributes with all the species to the community, whereas the others provide only a fraction (f) of their species. (left). Detail on the relative contribution of the species provided by each group; some species' abundance is set to 0 (italics red fonts) to increase β-diversity. Finally, the relative abundances are normalized (right).

TABLE 1 Vegetation radiative transfer model parameters, symbols, units, and bounds commonly found in the literature (see Supporting Information S1) used in the simulation.

Plant traits	Symbol	Units	Bounds
Leaf chlorophyll content	C_{ab}	$\mu g\,cm^{-2}$	[0, 100]
Leaf carotenoids content	C_{ca}	$\mu g\,cm^{-2}$	[0, 25]
Leaf anthocyanins content	C_{ant}	$\mu g\,cm^{-2}$	[0, 10]
Leaf senescent pigments content	C_s	a.u.	[0, 1]
Leaf water content	C_w	$g\,cm^{-2}$	[0.004, 0.045]
Leaf dry matter content	C_{dm}	$g\,cm^{-2}$	[0.00190, 0.01570]
Leaf structural parameter	N	layers	[1, 3]
Leaf area index	LAI	$m^2\,m^{-2}$	[0, 8]
Leaf inclination distribution function	$LIDF_a$	—	[−1, 1]; $\lvert LIDF_a + LIDF_b \rvert \le 1$
Bimodality of the leaf inclination	$LIDF_b$	—	
Canopy height	h_c	m	[0.1, 10.0]
Leaf width	l_w	m	[0.01, 0.1]

validated, respectively, with a look-up table of 6000 and 1000 pairs of reflectance factors between 400 and 2400 nm and model vegetation parameters (Table S2). In addition to species-dependent vegetation parameters, we randomly assigned soil parameters for each region, whereas atmospheric and illumination parameters and nadiral view were fixed for all the simulations (Table S3).

2.3 | Diversity indices and equivalent numbers

2.3.1 | Rao Q index and its equivalent number

The Rao Q entropy index expresses the expected dissimilarity (d) between two random samples from a population of N individuals of relative abundances p.

$$Q = \sum_{i,j}^{N} p_i p_j d_{ji}. \quad (1)$$

If $d_{ij}=1$ for all $i \neq j$ (the maximum dissimilarity) and $d_{ij}=0$ otherwise, Rao Q reduces to the Gini-Simpson index (Botta-Dukát, 2005). This definition is equivalent to the maximum attainable functional diversity, and the corresponding equivalent number (Q_{eq}) is (Jost, 2006):

$$Q_{eq} = \frac{1}{1-Q}. \quad (2)$$

de Bello et al. (2010) showed that this formulation is valid for Rao Q expressing functional or phylogenetic diversity if the dissimilarity metric is normalized between 0 and 1.

2.3.2 | Functional richness

We computed functional richness from the principal components (PC) selected using the Python function *ConvexHull*() from (SciPy

v1.8.0). Since the computational cost increases exponentially with dimensionality, the three first PCs are sometimes selected to compute FRic (Dahlin, 2016; Rossi et al., 2021b). As for the rest of the data, we retained the PCs explaining at least 98% of the variance. However, we limited the maximum number of PCs to 8 to reduce computation time and 3 ($FRic_3$) to understand the effects of this choice in previous works.

2.4 | Partitioning of α, β and γ components of diversity

2.4.1 | Diversity decomposition

Following de Bello et al. (2010), we transformed the Rao Q index into equivalent numbers and decomposed diversity (Equations 3–5) using Q and Q_{eq}. We calculated α-diversity extending Equation (2) to correct for differences in the number of communities within regions.

$$\alpha = \frac{1}{1 - \frac{1}{n_{com}} \sum_{i}^{n_{com}} Q_i}, \quad (3)$$

where n_{com} is the number of communities in the region, and Q_i is the Rao Q index or the equivalent number of each community. Following de Bello et al. (2010), we used the average of the Q metric and not the average α-diversity component. We computed γ-diversity using the Rao metric of all the region species with re-normalized relative abundances (Q_γ),

$$\gamma = \frac{1}{1 - Q_\gamma}. \quad (4)$$

We only calculated β-diversity using additive partition (Equation 5) since additive and multiplicative approaches are equivalent for Q_{eq} (de Bello et al., 2010),

$$\beta = \gamma - \alpha. \quad (5)$$

The fractions of γ-diversity represented by α (f_α) and β (f_β) components were calculated by dividing α and β by γ, respectively.

2.4.2 | Variance-based partitioning

Laliberté et al. (2020) proposed exploiting the variance of the spectral signals to partition the spectral diversity of a region (γ-diversity) into additive α (within communities) and β (among communities) components. The method partitions the sum of squares (SS) of a matrix of spectral variables representing a region (SS_{total}) into the within (SS_{within}) and the among-group (SS_{among}) components and can be summarized as follows:

$$SS_{total} = SS_{among} + SS_{within}, \quad (6)$$

$$\sum_{i=1}^{n}\sum_{j=1}^{p}(y_{ij} - \overline{y}_j)^2 = \sum_{k=1}^{q}\sum_{j=1}^{p} m(\hat{y}_{kj} - \overline{y}_j)^2 + \sum_{i=1}^{m}\sum_{k=1}^{q}\sum_{j=1}^{p}(y_{ij} - \hat{y}_{kj})^2, \quad (7)$$

where (following the original notation) p is the number of variables (i.e. PCs selected), n is the number of species or pixels of the region analysed, q is the number of communities among which variance is compared, and m is the number of samples in each group (abundance). y_{ij} refers to an individual element of the n-by-p matrix, $\overline{y}_j$ is the mean of each variable (i.e. PC), and $\hat{y}_{kj}$ is the corresponding k community mean.

Laliberté et al. (2020) method directly applies to images where each pixel i is a sample. However, our simulations (Sections 2.1 and 2.2) used relative abundances. Therefore, we adapted the method to partition diversity from a species-by-traits matrix and a matrix of relative abundances normalized per community. Also, we applied weighted PCA (Delchambre, 2015) implemented in the Python package WPCA (https://github.com/jakevdp/wpca) to ensure the abundance-weighted sum of squares of the PCA components was unbiased.

2.5 | Generalizable normalization approach

GN normalizes FDMs computed from PCs of standardized continuous variables whose dissimilarity metric is the Euclidean distance:

$$d_{ij} = \sqrt{\sum_{k=1}^{n_{var}} (x_{k,i} - x_{k,j})^2}, \quad (8)$$

where n_{var} is the number of continuous variables (x, plant traits or spectral), d_{ij} is the Euclidean distance between the variables of the species (or pixels) i and j.

Our rationale departs from the traits. If these range within physically or biologically plausible upper (b_{upper}) and lower (b_{lower}) bounds covering their variability in space and time, we can define a maximum plausible dissimilarity (d_{max}) directly from those bounds:

$$d_{max} = \sqrt{\sum_{k=1}^{n_{var}} (b_{upper,k,i} - b_{lower,k,j})^2}. \quad (9)$$

However, FDMs require standardizing x:

$$z = \frac{x - \mu}{\sigma}. \quad (10)$$

To calculate the maximum plausible dissimilarity of the z-scores ($d_{max,z}$) we redefine the bounds as the distance to the centred mean ($\mu = 0$) expressed as a number (n_σ) of standard deviations (σ) that cover most of a Normal distribution's probability. We chose $n_\sigma = 6$ covering more than 0.999999 of the data range, limiting exceeding variables to a minimum. These bounds are common to all variables,

$$d_{max,z} = \sqrt{\sum_{k=1}^{n_{var}} (2n_\sigma)^2}. \quad (11)$$

Furthermore, FDMs require reducing collinearity with PCA, where a transformation maps the *z*-scores to a new space of uncorrelated variables:

$$T = XW, \tag{12}$$

where T is the matrix of components and is orthogonal, X is the matrix of variables in the original space, and W is the matrix of basis vectors made of the eigenvectors of X's covariance matrix (Σ). W is calculated from Σ using, for example, eigendecomposition:

$$\Sigma W = \lambda v, \tag{13}$$

where λ are the eigenvalues, proportional to the variance explained by each eigenvector (W columns). PCA keeps the L columns of W that explain a given fraction of the total variance (f_{σ^2}). In this case, d_{max} cannot be generally calculated from the standardized bounds since projections differ for each dataset, and the projected bounds would not be generalizable. However, for any set of *z*-scores, the maximum Euclidean distance between PCs would be found if all the variables were orthogonal. In that case, Σ and the matrix of eigenvectors (W in Equation 12) equal the identity matrix (I), which enables the straightforward transformation of the (standardized) bounds (X_b):

$$T_b = X_b W_L = X_b I_L. \tag{14}$$

Therefore, the maximum Euclidean distance for any set of principal components ($d_{max,PCA}$) only depends on the number of PCs kept for X if it was orthogonal ($L^{\perp}$) and the *z*-score bounds:

$$d_{max,PCA} = \sqrt{\sum_{k=1}^{L^{\perp}} (2n_\sigma)^2}. \tag{15}$$

Since all the eigenvectors of an orthogonal matrix explain the same variance ($\lambda_i = 1$), $L^{\perp}$ will exclusively depend on f_{σ^2} and the number of variables in the original dataset. Additionally, we can use ceil rounding (notated as $]x[$) to obtain the integer number of components selected that explains at least the specified f_{σ^2},

$$d_{max,PCA} = 2n_\sigma \sqrt{]L^{\perp}[} = 2n_\sigma \sqrt{]n_{var} f_{\sigma^2}[}. \tag{16}$$

This approach also allows formulating a maximum value for the sum of squares (SS) of a set of PCs, used in the total variance diversity partitioning framework (Section 2.4.2), as the sum of the squared half-bound range of all the samples of the dataset (n_s):

$$SS_{max,PCA} = \sum_{k=1}^{n_s}]L^{\perp}[\cdot {n_\sigma}^2 = \sum_{k=1}^{n_s}]n_{var} f_{\sigma^2}[\cdot {n_\sigma}^2. \tag{17}$$

$SS_{max,PCA}$ could normalize the variance of different datasets when used to separate the spatial (Laliberté et al., 2020) or the spatial and temporal diversity components (Rossi et al., 2021a).

The approach can be expanded to FRic, the convex hull volume of the selected PCs. Its maximum plausible value would be the *n*-dimensional volume of a Euclidean hypersphere (NIST, 2013) of radius $r = n_\sigma f_{\sigma^2}$ in *n*-dimensional Euclidean space:

$$V_{max,PCA} = \frac{\pi^{\frac{L}{2}}}{\Gamma\left(\frac{L}{2}+1\right)} \left(n_\sigma f_{\sigma^2}\right)^L, \tag{18}$$

where Γ is the Gamma function, and L is the hypersphere's dimensionality. In this case, L equals the number of PCs retained from the dataset *z*-scores so that normalization can correct for the dependence of the hypersphere volume on L:

$$FRic_{norm} = \sqrt[L]{\frac{FRic}{V_{max,PCA}}}. \tag{19}$$

2.6 | Evaluation of the links between remote sensing and field plant trait information

We assessed the capability of local and generalizable normalization to:

1. Set diversity FDMs computed from RS variables and field plant traits to the same scale (data range). To do so, we adjusted linear models ($y = b_0 + b_1 x$) (Figure 1c). We would expect that two datasets with the same diversity cast the same values, and then the slope (b_1) would equal 1. However, this might not be the case due to non-linearities between plant traits and spectral variables (Pacheco-Labrador et al., 2022). Therefore, we also computed the averages' ratio ($\bar{y}/\bar{x}$) to assess to what extent, normalizations were able to set different variables at the same scale.
2. Keep or improve the strength of the correlations between RS and field FDMs via the squared Pearson correlation coefficient (r^2).
3. Produce similar FDM values and correlations for four different spectral configurations (number of bands and spectral range) representative of the main optical RS missions (Figure S2). The reference case was the reflectance factors at 1 nm step directly output from the model ('full-hyperspectral', Hy). Then we convolved full-hyperspectral spectra to the bands of the three RS missions: The DLR Earth Sensing Imaging Spectrometer (DESIS), Sentinel-2 (S2) Multi-Spectral Instrument, and QuickBird-2 (QB2). DESIS is a visible-to-near-infrared (VNIR) hyperspectral imager featuring 58 bands (4x binned) between 410 and 986 m. Sentinel-2 is one of the Copernicus missions managed by the European Space Agency (ESA) with 10 bands from the visible to the short-wave infrared (VSWIR). QuickBird-2 is a mission from Maxar (USA) and part of the ESA's Third Party Mission Programme. It carried the Ball Global Imagery System 2000 (BGIS2000), featuring four VNIR bands plus a panchromatic one. While no longer operative, it represents high spatial resolution missions.

3 | RESULTS

3.1 | Comparability of remote sensing and plant trait diversity estimates

GN increased the comparability between field PT and RS diversity metrics differently. Non-normalized $FRic_{non}$ presented large discrepancies (Figure 3a); local normalization limited $FRic_{local}$ values within the range [0, 1] and slightly increased r^2 (Figure 3d), whereas GN failed to provide comparable (1:1) $FRic_{GN}$ values but improved the correlation between RS and plant data (Figure 3h). Limiting the number of PCs to 3 led to stronger correlations (Figure 3b,e) and GN maximized r^2 without achieving 1:1 comparability (Figure 3i). For Rao Q (Figure 3c,f,j) and Q_{eq} (Figure 3g,k), local normalization reduced r^2 but brought values closer to the 1:1 line (Figure 3f,g). In contrast, GN kept the original r^2 for Rao Q (Figure 3j) and slightly reduced it for Q_{eq} (Figure 3k) while made field PT and RS metrics directly comparable.

GN also provided 1:1 comparable PT and RS values of the α-, β- and γ-diversity components estimated with Rao Q (Figure 4k–m), keeping the correlation from non-normalized indices (Figure 4a,b). Contrarily, local normalization reduced r^2 and led to higher averages' ratios for α and γ-diversity (Figure 4f–h). In all the cases, the fractions of α- and β-diversity remained the same (Figure 4d,e,i,j,n,o). Similarly, GN provided stronger and less biased correlations between diversity components (Figure 4u–w) than local normalization (Figure 4p–r) when using Q_{eq}. However, it strongly reduced the range of variability of the fractions of α and β-diversity (Figure 4s,t); overall, the relationships between RS and PT estimates were weaker than when computed with the indices. In all the cases, γ-diversity was the least correlated.

GN applied to the variance-based partition approach (i.e. Laliberté et al. (2020)) slightly improved the strength of the correlation between PT and RS estimates of α, β, and γ components, making them comparable in magnitude (Figure 5a–c vs. Figure 5k–m). On the contrary, local normalization (Figure 5f–h) reduced comparability and correlation.

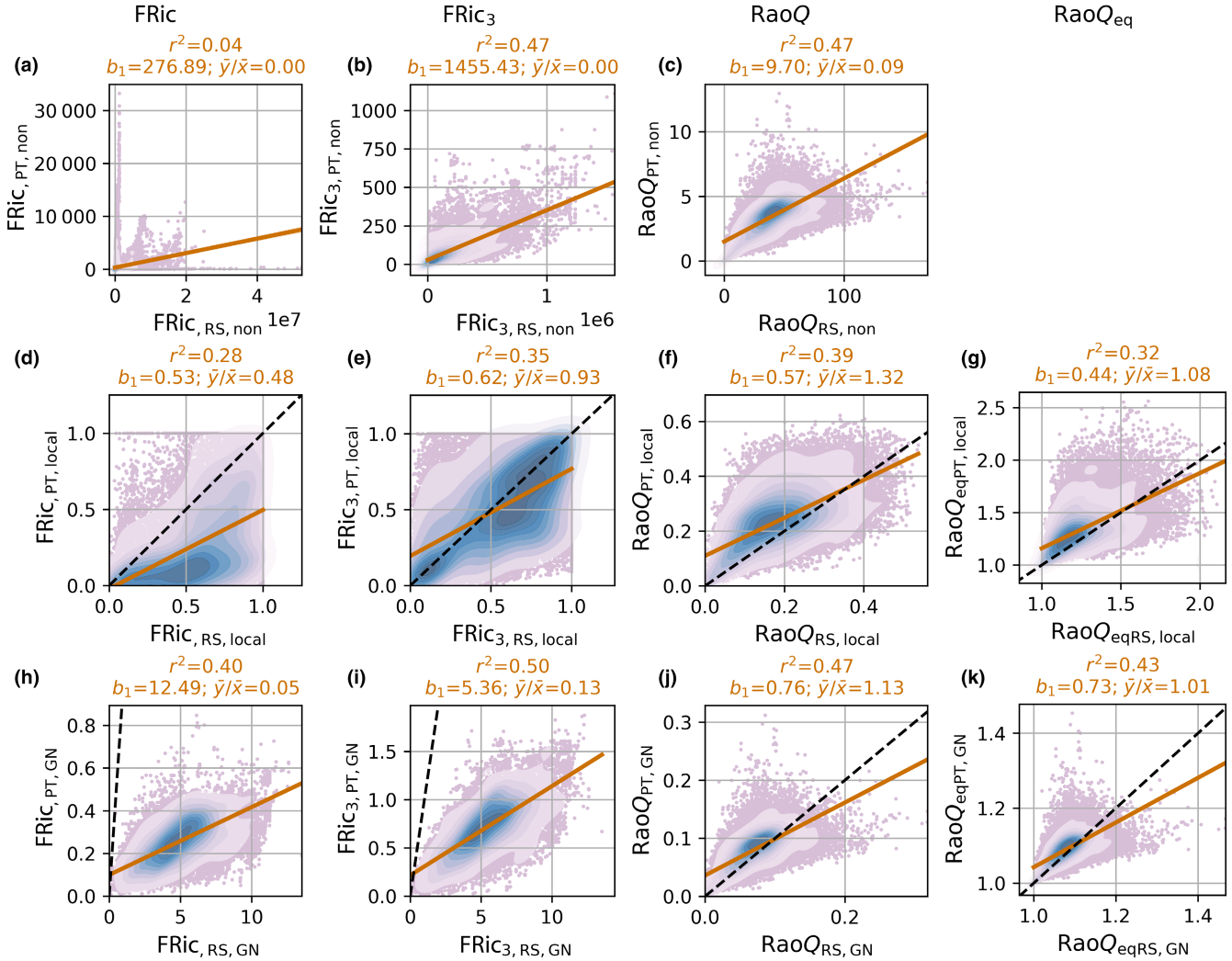

FIGURE 3 Diversity indices and equivalent numbers computed with non (first row), local (second row), and generalizable normalization (GN, third row) corresponding to field plant trait (*y*-axis) and full-hyperspectral remote sensing (*x*-axis) datasets. FRic (first column), FRic limited to up to three principal components (second column), Rao Q index (third column) and its equivalent number (fourth column). Squared Pearson correlation coefficient (r^2), the linear model slope (b_1), and the averages' ratio ($\bar{y}/\bar{x}$) are presented.

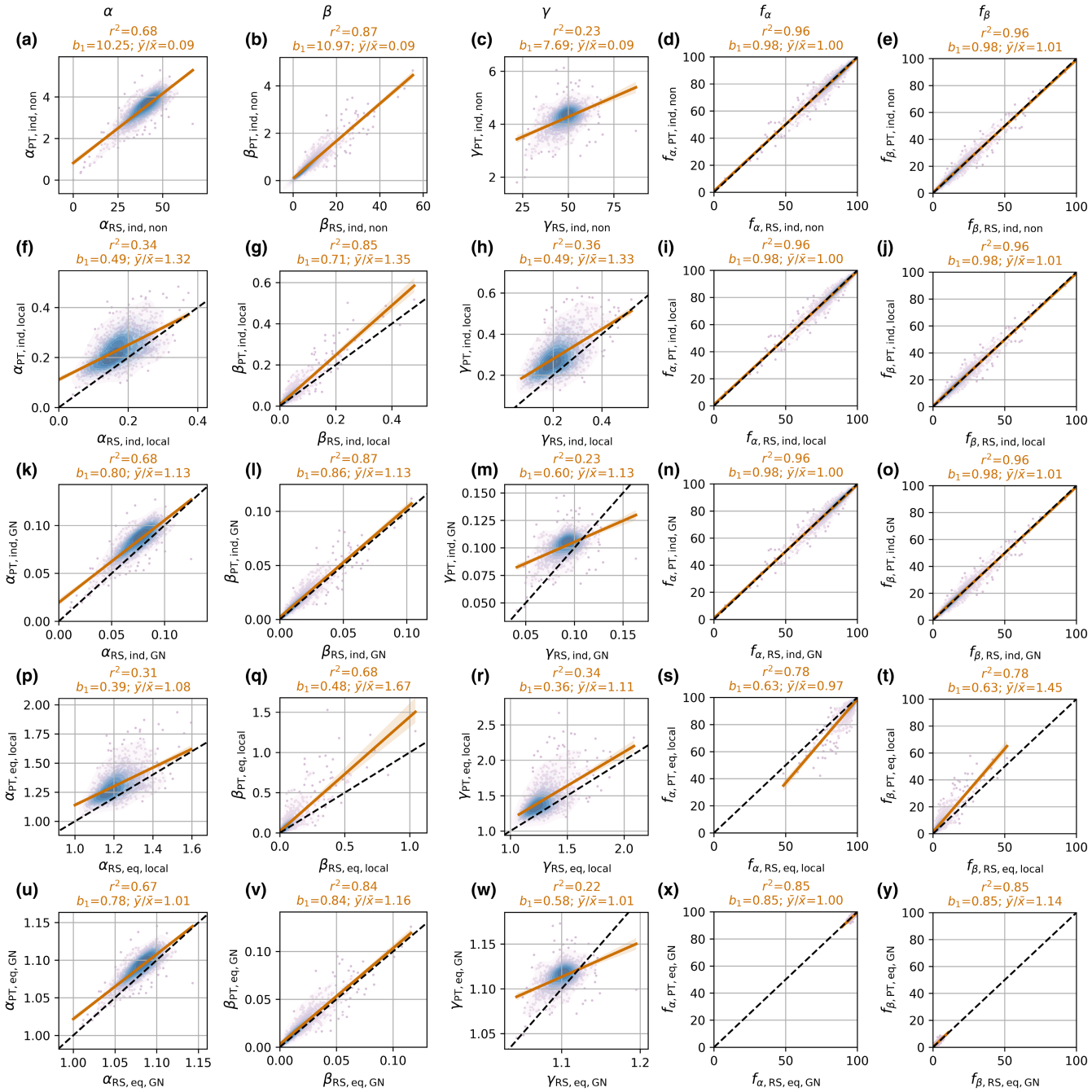

FIGURE 4 Diversity decomposition using the diversity index Rao Q with non- (first row), local (second row), and generalizable normalization (GN, third row), or its equivalent number with local (fourth row), and GN (fifth row) corresponding to field plant trait (*y*-axis) and full-hyperspectral remote sensing (*x*-axis) datasets. Estimates of α (first column), β (second column) and γ (third column) diversity, as well as the fractions of α (fourth column) and β (fifth column). Squared Pearson correlation coefficient (r^2), the linear model slope (b_1), and the averages' ratio ($\bar{y}/\bar{x}$) are presented.

Moreover, variance analysis accurately linked PT and RS γ-diversity, while it did not affect nor compress α and β-diversity fractions.

3.2 | Comparability across spectral configurations

Figure 6 summarizes the RS-PT comparison presented in the former section for different spectral configurations and the cases of non- and generalizable normalization. Sentinel-2 featured the largest r^2, followed by QB2 and DESIS for $FRic_{non}$ (Figure 6a–c), whereas GN made the different sensors' r^2 larger and more similar. For $FRic_3$, full-hyperspectral presented the second largest r^2; however, GN barely modified correlation strength and did not achieve direct comparability of FRic and $FRic_3$ for none of the missions evaluated. Even after GN, the sensors with more bands deviated most from the unit model slope (Figure 6b) and averages' ratio (Figure 6c). In

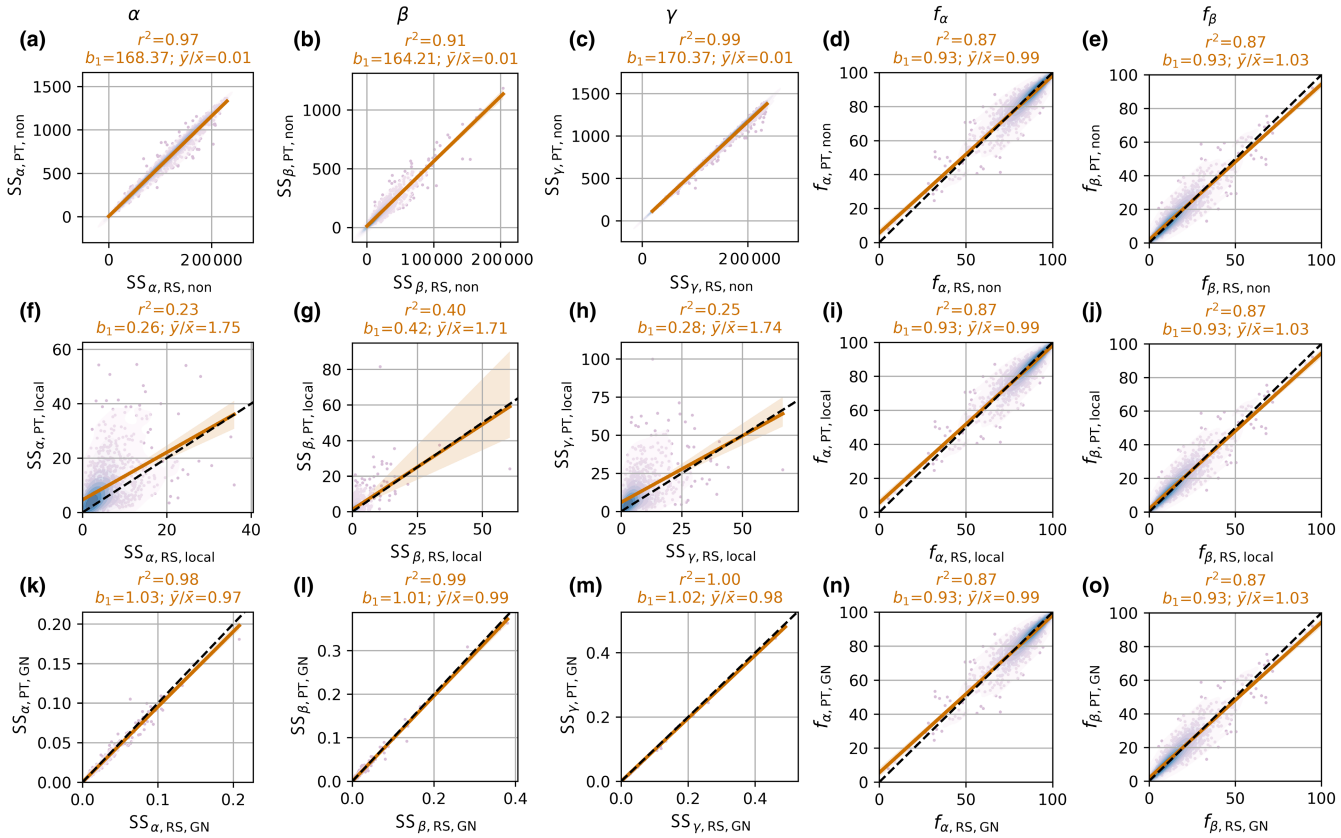

FIGURE 5 Diversity decomposition using variance without (first row), with local (second row), and generalizable normalization (GN, third row) corresponding to field plant trait (*y*-axis) and full-hyperspectral remote sensing (*x*-axis) datasets. Estimates of α (first column), β (second column), and γ (third column) components, as well as the fractions of α (fourth column) and β (fifth column). Squared Pearson correlation coefficient (r^2), the linear model slope (b_1), and the averages' ratio ($\bar{y}/\bar{x}$) are presented.

contrast, the VSWIR sensors achieved the strongest relationships once normalized. GN did not modify Rao *Q* correlation but strongly reduced sensor differences in slope and averages' ratio, making them closer to 1 and, therefore, more directly comparable. As with FRic, S2 presented the highest r^2 before and after normalization. Q_{eq} was computed only after normalization; correlations were slightly weaker than for *Q* (Figure 6a), but the slopes and especially averages' ratios were similar and close to 1 (Figure 6b,c). Diversity decomposition showed that GN did not modify r^2 except for α and β fractions when applied to Q_{eq} (Figure 6d), which deviated from the 1:1 relationship (Figure 6e,f). For the rest of the cases, GN homogenized the relationships for the different sensors, leading to similar slopes and similar and close-to-unity averages' ratios (Figure 6d–f). β and γ-diversity showed the strongest and the weakest RS-PT correlations, respectively. As before, VNIR sensors presented lower r^2 than VSWIR sensors, whereas, without normalization, S2 estimates were the closest to the PT α, β, and γ components, followed by QB2. Results were similar for variance-based partitioning (Figure 6g–i). The lack of normalization made the metrics not directly comparable, whereas S2 and QB2 showed the closest results to PT. However, GN strongly homogenized RS estimates. Furthermore, it improved the correlation of β diversity while barely modifying r^2 for the rest of the components, which were slightly better for VSWIR sensors. The variance-based partitioning offered stronger correlations between the γ-diversity than Rao *Q* decomposition but weaker for α and β-diversity fractions, unaffected by the normalization.

4 | DISCUSSION

The proposed GN enabled the direct comparison (1:1) of FDMs (Rao *Q* and SS) and diversity components (α, β, and γ) computed from field plant traits and different remote sensors (first research question), keeping or increasing their correlation (second research question). Contrarily, the local normalization approach proved not suitable for RS. GN removes data-structure effects from biodiversity information, casting similar FDM values for heterogeneous datasets of similar diversity but different numbers of correlated variables (Figure S1). Former works sought to bridge methods (Chao & Chiu, 2016) or outbalance autocorrelation (de Bello, Botta-Dukát, et al., 2021), but to our knowledge, no similar normalization has been proposed. The problem addressed might be less acute in ecology, where survey costs prevent the oversampling that RS can achieve, and technical challenges relate to aggregating numerous inhomogeneous databases (Anderson et al., 2020; De Palma et al., 2018). However, RS brings its own challenges and methodological questions, such as data

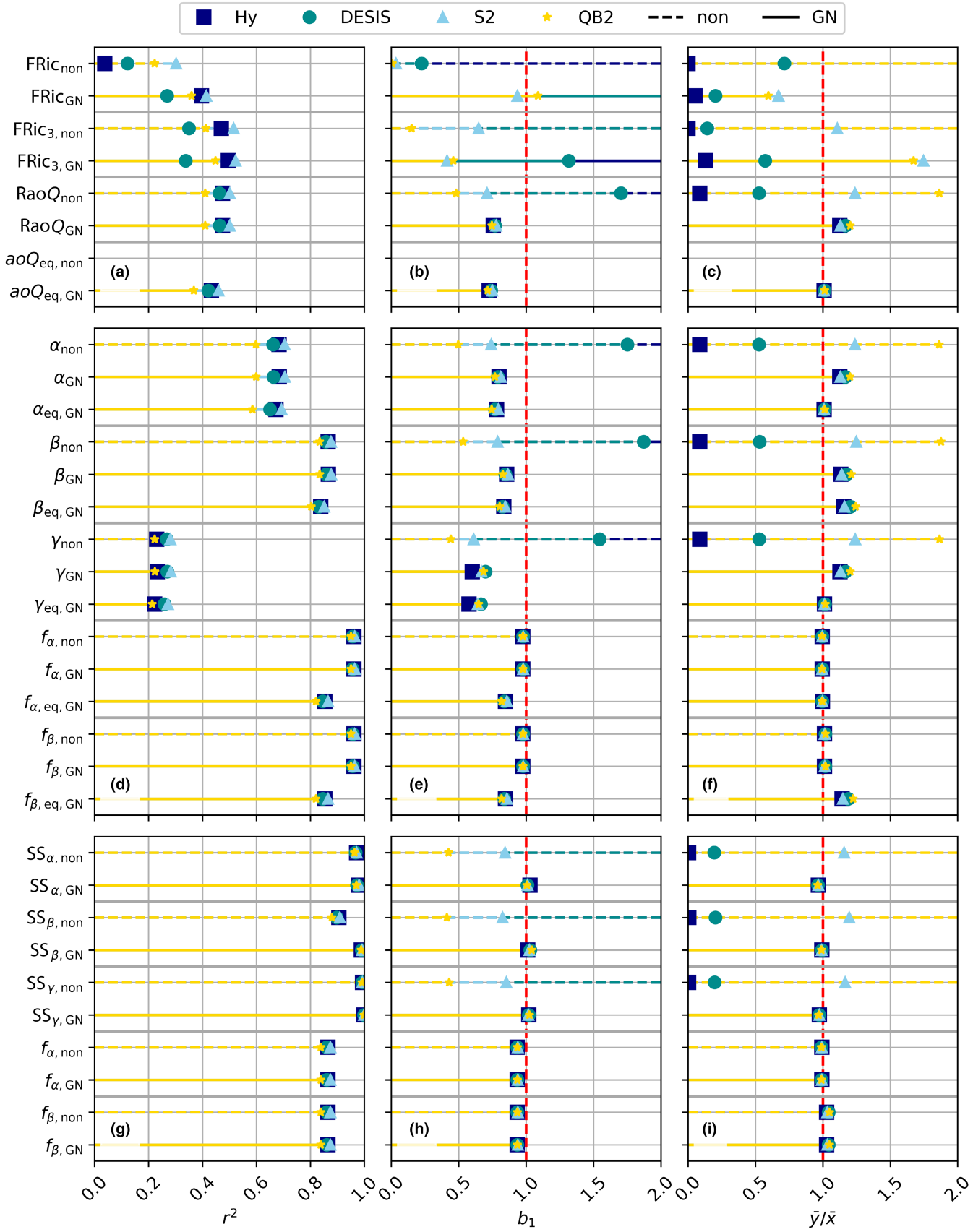

FIGURE 6 Comparison of remote sensing and plant trait functional diversity metrics (a–c), diversity decomposition (d–f), and variance-based diversity partitioning (g–i) with non and generalizable normalization for different spectral configurations: Full-hyperspectral (Hy), DESIS, Sentinel-2 (S2), and Quick Bird 2 (QB2). Squared Pearson correlation coefficient (r^2), the linear model slope (b_1), and the averages' ratio ($\overline{y}/\overline{x}$) are presented; the red dashed line indicates unity. Assessment of functional richness (FRic), Rao quadratic entropy (Q), its equivalent number (Q_{eq}), the α, β, and γ-diversity components, as well as the fractions of α and β.

volume, sensors' diversity, or the validation of PFD estimates. In RS, normalization has only been applied in self-normalized metrics (e.g. functional divergence or evenness) using a local approach (Schneider et al., 2017; Wang, Gamon, Schweiger, et al., 2018), which makes them not comparable across images (Pacheco-Labrador et al., 2022). GN removes the confusion brought by the variability of spectral configurations and can be applied to heterogeneous field data to improve validation capabilities. Moreover, GN is data-agnostic since it does not require exploring the entire dataset to estimate the maximum dissimilarity, making comparable metrics computed independently. We suggest GN as a necessary step toward developing interpretable global-coverage maps of PFD.

GN does not solve other RS limitations to infer PFD assessed in previous studies, such as spatial and temporal mismatches, resolution, trait retrieval uncertainty, or signal noise (Helfenstein et al., 2022; Pacheco-Labrador et al., 2022; Rossi et al., 2021b). These issues affect PFD estimation before normalization. Furthermore, while local normalization dependence on the maximum dissimilarity observed can increase the uncertainty of the normalized metrics, the data-agnostic GN prevents further uncertainty propagation. We evaluated the new approach using a simulation framework similar to the one developed and validated by Pacheco-Labrador et al. (2022), who also discussed the use of specific radiative transfer models (i.e. SCOPE) and the computation of PFD from their inputs. As before, modelling conditions affect the estimation of PFD but not the GN itself. While our simulations ensure the correlation of spectral and PFD (noiseless, full spatial resolution), testing less ideal conditions led to no additional effects on the normalization (e.g. non- and GN featured the same r^2 between RS and PT data, not shown).

GN failed to make FRic comparable, but it improved the RS-PT correlations (Figure 3). Despite explaining less variance, limiting the number of components ($FRic_3$) increased the RS-PT r^2. Contrarily, the method provides comparable Rao Q indices and equivalent numbers (Figure 3), the latest unexplored in RS, which offers a more direct interpretation and comparability of diversity estimates. GN led to comparable and similarly correlated Q, Q_{eq} and respective α-, β- and γ-diversity. Equivalent numbers are supposed to prevent spurious underestimation of β-diversity (Jost, 2007); de Bello et al. (2010) found f_β increased when using only two functional traits. Contrarily, we found a substantial reduction of f_β both for PT and spectral datasets (Figure 4), but we also used datasets of much larger dimensionality. We hypothesize that large dimensionality makes it unlikely that many species are maximally dissimilar for numerous traits, leading to small normalized Q, large Q_{eq} (Equation 2) and, therefore, α-diversity and f_α. Variance-based diversity partitioning provided stronger correlations (r^2) between RS and PT estimates and in particular for α- and γ-diversity (Figure 5), which were consistently lower when computed from Rao Q (Figure 4). On the contrary, the relationships between the fractions of α- and β-diversity were less precise. Variance analysis was also computationally faster (~140 times) since it does not require comparing all the species.

GN already provided insight into the relationships between spectral and PFD in this work. RS and PT Rao Q are centered ($\bar{y}/\bar{x} \sim 1$); but biased ($b_1 < 1$). Former studies could only assess the correlation but not understand whether RS under or overestimated PFD (Hauser, Féret, et al., 2021; Torresani et al., 2019). While the Spectral Variation Hypothesis has been validated for functional diversity (Pacheco-Labrador et al., 2022; Torresani et al., 2019), we do not know whether spectral diversity should equal PFD. GN allows us to hypothesize that they might not be due to non-linearities and saturating absorption or scattering (Pacheco-Labrador et al., 2022), background (Hauser, Timmermans, et al., 2021; Wang, Gamon, Schweiger, et al., 2018) or directional effects. We also found that species richness and β-diversity affect the correlations between PT and RS metrics. Pacheco-Labrador et al. (2022) simulated a maximum of 30 species, and FRic and Rao Q indices presented $r^2 \sim 0.61$ and 0.75, respectively. Here, $S_{reg} = 300$ led to lower r^2 (0.04 and 0.47, Figure 3); repeating the simulations with $S_{reg} = 30$ increased r^2 to 0.22 and 0.66, respectively (Figure S3). Furthermore, during Rao Q diversity decomposition, lower species richness increased r^2 for α and γ but reduced it for β-diversity (Figure S4). In contrast, correlations decreased for all the diversity metrics in the variance-based diversity partitioning (Figure S5). These results suggest that the size of the plots/moving windows used for analysis (and therefore the S_{reg} comprised) influences these correlations. While the relationship area-diversity has been explored in RS (Dahlin, 2016; Helfenstein et al., 2022; Schneider et al., 2017), the effect of the area on the RS-PT diversity relationships has not been analysed. Combining and comparing several approaches—facilitated by GN—might contribute to identifying uncertainties and understanding such relationships.

GN can improve the interpretation and comparison of RS and field FDMs. For example, S2 and PT metrics were closely comparable in the simulations before normalization, suggesting that S2 is better suited for this application than other sensors (Figure 5g–l). However, global normalization revealed that such comparability resulted from the similar dimensionality of the datasets (10 and 12 variables). Results would differ for field datasets featuring fewer PT, which is often the case (Hauser, Féret, et al., 2021; Schneider et al., 2017). Also, VSWIR sensors better captured PFD than VNIR ones (larger r^2) since SWIR radiation is affected by foliar dry matter and water contents; however, similar slopes for all sensors indicate no systematic underestimation of PFD from VNIR sensors.

Biodiversity monitoring would benefit from multi-mission products compensating for individual spectral, spatial, and temporal resolution or thematic information deficiencies. GN allows directly combining and analysing FDMs issued from heterogeneous datasets and, therefore: (1) Combining multi-mission RS imagery to analyse spatial resolution effects on a global scale (so far limited to local; Helfenstein et al., 2022; Schneider et al., 2017) and optimize correction and data-fusion approaches. (2) Integrating lidar, radar, thermal, or sun-induced chlorophyll fluorescence data to exploit more structurally and physiologically-driven information (e.g.

Tagliabue et al. (2020)). (3) Mixing vegetation products (e.g. plant trait estimates) and spectroradiometric data. Pacheco-Labrador et al. (2022) showed that plant trait estimates correlated more than reflectance factors with PFD; since they accounted for confounding effects (e.g. background); but were sensitive to retrieval uncertainties. Thus, their combination could improve robustness and identify uncertain PFD estimates. (4) Through meta-analysis, integrating RS and heterogeneous vegetation datasets to decipher hidden relationships between spectral diversity and the diversity of plant traits with no physical link (e.g. root traits). (5) Comparing heterogeneous PT datasets to assess the information carried by different traits of interest in ecological research. In this context, GN would help to understand, but not solve, the differences in information content presented by observations generated with different physical mechanisms (e.g. optical, radar, lidar) and with different spatial resolutions and angular configurations. Further research will be required to interpret or remove confounding factors from the information on PFD.

5 | CONCLUSIONS

We proposed a generalizable normalization approach that enables the comparability of Rao's quadratic entropy indices, equivalent numbers, and diversity components independently of the spectral configuration of the remote sensor or the number of field plant traits analysed. Since it provides data-structure-independent metrics, their comparison depends only on the diversity-information content and the quality of the datasets. The approach enables the integration of heterogeneous datasets for global monitoring of PFD from space and validating these new products; it might allow a better understanding of the capability and complementarity of the different missions to capture PFD. Generalizable normalization demonstrated that functional diversity metrics from plant trait and spectral information correlate but are unequal. Furthermore, species richness and β-diversity affect their comparison.

AUTHOR CONTRIBUTIONS

Javier Pacheco-Labrador: conceptualization, investigation, writing—original draft, visualization; **Javier Pacheco-Labrador, Francesco de Bello and Mirco Migliavacca**: methodology, formal analysis; **Xuanlong Ma, Mirco Migliavacca and Christian Wirth**: Funding acquisition; **Javier Pacheco-Labrador and Mirco Migliavacca**: Project administration; **Javier Pacheco-Labrador, Francesco de Bello, Mirco Migliavacca, Xuanlong Ma, Nuno Carvalhais and Christian Wirth**: Writing—review & editing.

ACKNOWLEDGEMENTS

Javier Pacheco-Labrador, Mirco Migliavacca, Xuanlong Ma, and Christian Wirth acknowledge the German Aerospace Center (DLR) project OBEF-Accross2 'The Potential of Earth Observations to Capture Patterns of Biodiversity' (contract no. 50EE1912, German Aerospace Center). Javier Pacheco-Labrador was funded by the ESA Living Planet Fellowship IRS4BEF 'Integrated Remote Sensing for Biodiversity-Ecosystem Function' (C.N.4000140028/22/I-DT-lr). Francesco de Bello was supported by the Valencian Community project CIAICO/2021/181. We thank Prof. Dr. Miguel Mahecha for his support and fruitful discussions. Open Access funding enabled and organized by Projekt DEAL.

CONFLICT OF INTEREST STATEMENT

The authors declare no conflict of interest.

PEER REVIEW

The peer review history for this article is available at https://www.webofscience.com/api/gateway/wos/peer-review/10.1111/2041-210X.14163.

DATA AVAILABILITY STATEMENT

The Python package pyGNDiv performing the simulations and applying non, local, and generalizable normalization is publicly available in Zenodo repository (Pacheco-Labrador, 2023).

ORCID

Javier Pacheco-Labrador https://orcid.org/0000-0003-3401-7081
Francesco de Bello https://orcid.org/0000-0001-9202-8198
Mirco Migliavacca https://orcid.org/0000-0003-3546-8407
Xuanlong Ma https://orcid.org/0000-0003-1499-8476
Nuno Carvalhais https://orcid.org/0000-0003-0465-1436

REFERENCES

Anderson, R. P., Araújo, M. B., Guisan, A., Lobo, J. M., Martínez-Meyer, E., Peterson, A. T., & Soberón, J. M. (2020). Optimizing biodiversity informatics to improve information flow, data quality, and utility for science and society. *Frontiers of Biogeography*, *12*, 14. https://doi.org/10.21425/F5FBG47839

Botta-Dukát, Z. (2005). Rao's quadratic entropy as a measure of functional diversity based on multiple traits. *Journal of Vegetation Science*, *16*, 533–540.

Cavender-Bares, J., Gamon, J. A., Hobbie, S. E., Madritch, M. D., Meireles, J. E., Schweiger, A. K., & Townsend, P. A. (2017). Harnessing plant spectra to integrate the biodiversity sciences across biological and spatial scales. *American Journal of Botany*, *104*, 966–969.

Chao, A., & Chiu, C.-H. (2016). Bridging the variance and diversity decomposition approaches to beta diversity via similarity and differentiation measures. *Methods in Ecology and Evolution*, *7*, 919–928. https://doi.org/10.1111/2041-210X.12551

Dahlin, K. M. (2016). Spectral diversity area relationships for assessing biodiversity in a wildland–agriculture matrix. *Ecological Applications*, *26*, 2758–2768.

de Bello, F., Botta-Dukát, Z., Lepš, J., & Fibich, P. (2021). Towards a more balanced combination of multiple traits when computing functional differences between species. *Methods in Ecology and Evolution*, *12*, 443–448.

de Bello, F., Carmona, C. P., Dias, A. T. C., Götzenberger, L., Moretti, M., & Berg, M. P. (2021). *Handbook of trait-based ecology: From theory to R tools*. Cambridge University Press.

de Bello, F., Lavergne, S., Meynard, C. N., Lepš, J., & Thuiller, W. (2010). The partitioning of diversity: Showing Theseus a way out of the labyrinth. *Journal of Vegetation Science*, *21*, 992–1000.

De Boeck, H. J., Bloor, J. M. G., Kreyling, J., Ransijn, J. C. G., Nijs, I., Jentsch, A., & Zeiter, M. (2018). Patterns and drivers of biodiversity–stability relationships under climate extremes. *Journal of Ecology*, *106*, 890–902. https://doi.org/10.1111/1365-2745.12897

De Palma, A., Sanchez-Ortiz, K., Martin, P. A., Chadwick, A., Gilbert, G., Bates, A. E., Börger, L., Contu, S., Hill, S. L. L., & Purvis, A. (2018). Chapter four—Challenges with inferring how land-use affects terrestrial biodiversity: Study design, time, space and synthesis. In D. A. Bohan, A. J. Dumbrell, G. Woodward, & M. Jackson (Eds.), *Advances in ecological research* (pp. 163–199). Academic Press.

Delchambre, L. (2015). Weighted principal component analysis: A weighted covariance eigendecomposition approach. *Monthly Notices of the Royal Astronomical Society*, *446*, 3545–3555.

Gómez-Dans, J. L., Lewis, P. E., & Disney, M. (2016). Efficient emulation of radiative transfer codes using gaussian processes and application to land surface parameter inferences. *Remote Sensing*, *8*, 119.

Hansen, A. J., Noble, B. P., Veneros, J., East, A., Goetz, S. J., Supples, C., Watson, J. E. M., Jantz, P. A., Pillay, R., Jetz, W., Ferrier, S., Grantham, H. S., Evans, T. D., Ervin, J., Venter, O., & Virnig, A. L. S. (2021). Toward monitoring forest ecosystem integrity within the post-2020 global biodiversity framework. *Conservation Letters*, *14*, e12822.

Hauser, L. T., Féret, J.-B., An Binh, N., van der Windt, N., Sil, Â. F., Timmermans, J., Soudzilovskaia, N. A., & van Bodegom, P. M. (2021). Towards scalable estimation of plant functional diversity from Sentinel-2: In-situ validation in a heterogeneous (semi-)natural landscape. *Remote Sensing of Environment*, *262*, 112505.

Hauser, L. T., Timmermans, J., van der Windt, N., Sil, Â. F., César de Sá, N., Soudzilovskaia, N. A., & van Bodegom, P. M. (2021). Explaining discrepancies between spectral and in-situ plant diversity in multispectral satellite earth observation. *Remote Sensing of Environment*, *265*, 112684.

Helfenstein, I. S., Schneider, F. D., Schaepman, M. E., & Morsdorf, F. (2022). Assessing biodiversity from space: Impact of spatial and spectral resolution on trait-based functional diversity. *Remote Sensing of Environment*, *275*, 113024. https://doi.org/10.1016/j.rse.2022.113024

Hill, M. O. (1973). Diversity and evenness: A unifying notation and its consequences. *Ecology*, *54*, 427–432.

Jost, L. (2006). Entropy and diversity. *Oikos*, *113*, 363–375.

Jost, L. (2007). Partitioning diversity into independent alpha and beta components. *Ecology*, *88*, 2427–2439.

Khare, S., Latifi, H., & Rossi, S. (2019). Forest beta-diversity analysis by remote sensing: How scale and sensors affect the Rao's Q index. *Ecological Indicators*, *106*, 105520.

Laliberté, E., & Legendre, P. (2010). A distance-based framework for measuring functional diversity from multiple traits. *Ecology*, *91*, 299–305.

Laliberté, E., Schweiger, A. K., & Legendre, P. (2020). Partitioning plant spectral diversity into alpha and beta components. *Ecology Letters*, *23*, 370–380.

Ma, X., Migliavacca, M., Wirth, C., Bohn, J. F., Huth, A., Richter, R., & Mahecha, D. M. (2020). Monitoring plant functional diversity using the reflectance and echo from space. *Remote Sensing*, *12*, 1248. https://doi.org/10.3390/rs12081248

Mason, N. W. H., Mouillot, D., Lee, W. G., & Wilson, J. B. (2005). Functional richness, functional evenness and functional divergence: The primary components of functional diversity. *Oikos*, *111*, 112–118.

NIST. (2013). *Equation 5.19.4*. NIST Digital Library of Mathematical Functions.

Pacheco-Labrador, J. (2023). pyGNDiv described in Pacheco-Labrador et al. 2023. *Zenodo*, https://doi.org/10.5281/zenodo.7997302

Pacheco-Labrador, J., Migliavacca, M., Ma, X., Mahecha, M. D., Carvalhais, N., Weber, U., Benavides, R., Bouriaud, O., Barnoaiea, I., Coomes, D. A., Bohn, F. J., Kraemer, G., Heiden, U., Huth, A., & Wirth, C. (2022). Challenging the link between functional and spectral diversity with radiative transfer modeling and data. *Remote Sensing of Environment*, *280*, 113170.

Palmer, M. W., Earls, P. G., Hoagland, B. W., White, P. S., & Wohlgemuth, T. (2002). Quantitative tools for perfecting species lists. *Environmetrics*, *13*, 121–137.

Pearson, K. (1901). LIII. On lines and planes of closest fit to systems of points in space. *The London, Edinburgh, and Dublin Philosophical Magazine and Journal of Science*, *2*, 559–572.

Ricotta, C., & Szeidl, L. (2009). Diversity partitioning of Rao's quadratic entropy. *Theoretical Population Biology*, *76*, 299–302. https://doi.org/10.1016/j.tpb.2009.10.001

Rocchini, D., Luque, S., Pettorelli, N., Bastin, L., Doktor, D., Faedi, N., Feilhauer, H., Féret, J.-B., Foody, G. M., Gavish, Y., Godinho, S., Kunin, W. E., Lausch, A., Leitão, P. J., Marcantonio, M., Neteler, M., Ricotta, C., Schmidtlein, S., Vihervaara, P., … Nagendra, H. (2018). Measuring β-diversity by remote sensing: A challenge for biodiversity monitoring. *Methods in Ecology and Evolution*, *9*, 1787–1798.

Rocchini, D., Marcantonio, M., Da Re, D., Bacaro, G., Feoli, E., Foody, G. M., Furrer, R., Harrigan, R. J., Kleijn, D., Iannacito, M., Lenoir, J., Lin, M., Malavasi, M., Marchetto, E., Meyer, R. S., Moudry, V., Schneider, F. D., Šímová, P., Thornhill, A. H., … Ricotta, C. (2021). From zero to infinity: Minimum to maximum diversity of the planet by spatio-parametric Rao's quadratic entropy. *Global Ecology and Biogeography*, *30*, 1153–1162.

Rossi, C., Kneubühler, M., Schütz, M., Schaepman, M. E., Haller, R. M., & Risch, A. C. (2021a). Remote sensing of spectral diversity: A new methodological approach to account for spatio-temporal dissimilarities between plant communities. *Ecological Indicators*, *130*, 108106.

Rossi, C., Kneubühler, M., Schütz, M., Schaepman, M. E., Haller, R. M., & Risch, A. C. (2021b). Spatial resolution, spectral metrics and biomass are key aspects in estimating plant species richness from spectral diversity in species-rich grasslands. *Remote Sensing in Ecology and Conservation*, *8*, 297–314. https://doi.org/10.1002/rse2.244

Schneider, F. D., Morsdorf, F., Schmid, B., Petchey, O. L., Hueni, A., Schimel, D. S., & Schaepman, M. E. (2017). Mapping functional diversity from remotely sensed morphological and physiological forest traits. *Nature Communications*, *8*, 1441.

Stier, A. C., Bolker, B. M., & Osenberg, C. W. (2016). Using rarefaction to isolate the effects of patch size and sampling effort on beta diversity. *Ecosphere*, *7*, e01612.

Tagliabue, G., Panigada, C., Celesti, M., Cogliati, S., Colombo, R., Migliavacca, M., Rascher, U., Rocchini, D., Schüttemeyer, D., & Rossini, M. (2020). Sun–induced fluorescence heterogeneity as a measure of functional diversity. *Remote Sensing of Environment*, *247*, 111934.

Torresani, M., Feilhauer, H., Rocchini, D., Féret, J.-B., Zebisch, M., & Tonon, G. (2021). Which optical traits enable an estimation of tree species diversity based on the spectral variation hypothesis? *Applied Vegetation Science*, *24*, e12586.

Torresani, M., Rocchini, D., Sonnenschein, R., Zebisch, M., Marcantonio, M., Ricotta, C., & Tonon, G. (2019). Estimating tree species diversity from space in an alpine conifer forest: The Rao's Q diversity index meets the spectral variation hypothesis. *Ecological Informatics*, *52*, 26–34. https://doi.org/10.1016/j.ecoinf.2019.04.001

van der Tol, C., Verhoef, W., Timmermans, J., Verhoef, A., & Su, Z. (2009). An integrated model of soil-canopy spectral radiances, photosynthesis, fluorescence, temperature and energy balance. *Biogeosciences*, *6*, 3109–3129.

Wang, R., & Gamon, J. A. (2019). Remote sensing of terrestrial plant biodiversity. *Remote Sensing of Environment*, *231*, 111218.

Wang, R., Gamon, J. A., Cavender-Bares, J., Townsend, P. A., & Zygielbaum, A. I. (2018). The spatial sensitivity of the spectral diversity–biodiversity relationship: An experimental test in a prairie grassland. *Ecological Applications*, *28*, 541–556.

Wang, R., Gamon, J. A., Schweiger, A. K., Cavender-Bares, J., Townsend, P. A., Zygielbaum, A. I., & Kothari, S. (2018). Influence of species

richness, evenness, and composition on optical diversity: A simulation study. *Remote Sensing of Environment*, *211*, 218–228.
Whittaker, R. H. (1960). Vegetation of the Siskiyou Mountains, Oregon and California. *Ecological Monographs*, *30*, 279–338.
Whittaker, R. H. (1972). Evolution and measurement of species diversity. *Taxon*, *21*, 213–251. https://doi.org/10.2307/1218190

SUPPORTING INFORMATION

Additional supporting information can be found online in the Supporting Information section at the end of this article.

Data S1: Supplementary figures, tables and contents.

How to cite this article: Pacheco-Labrador, J., de Bello, F., Migliavacca, M., Ma, X., Carvalhais, N., & Wirth, C. (2023). A generalizable normalization for assessing plant functional diversity metrics across scales from remote sensing. *Methods in Ecology and Evolution*, *14*, 2123–2136. https://doi.org/10.1111/2041-210X.14163